Particle-in-cell techniques for the study of space charge effects in an electrostatic ion beam trap

Dhanoj Gupta, Raj Singh, Ryan Ringle, Catherine R. Nicoloff, Igor Rahinov, Oded Heber, and Daniel Zajfman

Phys. Rev. E **104**, 065202 — Published 9 December 2021

DOI: 10.1103/PhysRevE.104.065202

Particle-in-Cell Techniques for the study of space charge effects in an Electrostatic Ion Beam Trap

Dhanoj Gupta,[1,*] Raj Singh,[2] Ryan Ringle,[3,4] Catherine R. Nicoloff,[3,4] Igor Rahinov,[5] Oded Heber,[1,†] and Daniel Zajfman[1]

[1] *Department of Particle Physics and Astrophysics, Weizmann Institute of Science, Rehovot 7610001, Israel*
[2] *CIMAP, Ganil, Caen 14000, France*
[3] *Facility for Rare Isotope Beams, East Lansing, MI, USA*
[4] *Department of Physics and Astronomy, Michigan State University, East Lansing, MI, USA*
[5] *Department of Natural Sciences, The Open University of Israel, Raanana 4353701, Israel*

Abstract: We developed a simulation technique to study the effect of space charge interaction between trapped ions in the electrostatic ion beam trap (EIBT). The importance of space charge is demonstrated in both the dispersive and the self-bunching regime of the ion trap. The simulation results provide an estimate for the space charge effect on the trapping efficiency. They also allow for a better understanding of the enhanced diffusion and the self-bunching effect, and provide a better characterization of the EIBT as a mass spectrometer where, peak coalescence is important. The numerical results reproduce all experimental data, demonstrating the critical importance of including space charge effects, even at low ion density, in order to understand the ion trap dynamics.

I. INTRODUCTION

The electrostatic ion beam trap (EIBT), ever since its invention by Zajfman and co-workers [1, 2], has been an important development in the field of ion beam trapping, allowing for various applications in the field of atomic, molecular, and cluster physics [3]. The basic principle behind the EIBT is quite similar to that of the optical resonator [4]. Instead of optical mirrors, the EIBT electrostatic mirrors and lenses are used for trapping oscillating ions (see Figure 1). In a typical EIBT setup, a bunch of ions is introduced into the trap with a kinetic energy of a few keV. Once trapped, the ions oscillate between the two mirrors with a frequency in the range of hundreds of kHz. Trapping life time is mostly limited by the rate of collisions between the trapped ions and the residual gas, and for high number of trapped ions, also by ion-ion collisions induced by space charge.

The behavior of ions trapped in the EIBT is known to be strongly influenced by the values of the potentials on the mirror electrodes, as well as by space charge. The electrostatic potential on the mirrors can be tuned mainly in two modes: the dispersive or the self-bunching (synchronized) mode [5]. The critical parameter characterizing these two modes is the slip factor defined as

$$\eta = -\frac{2E_k}{f_{osc}}\frac{df_{osc}}{dE_k}, \tag{1}$$

where f_{osc} is the oscillation frequency of a trapped ion with initial kinetic energy E_k. When the slip factor is tuned to be negative, the mode is called dispersive mode. In this mode, the initial ion bunch spreads out rapidly. If the ion-ion interaction is strong (i.e., for a high density initial bunch), the diffusion process is even more enhanced for the same initial conditions [6]. When the slip factor is positive (meaning that slower ions oscillate with higher frequency), and the charge density is high enough, the overall dynamics result in the self-bunching of the ions, cancelling the dispersion. In this mode, the repulsive Coulomb interactions between the ions is the leading cause for the self-bunching phenomena [7]. A minimum ion density is required for creating long-lived stable bunches [8] in this mode. This unique feature has lead to some initial applications in the field of high-resolution Fourier transform mass spectrometry [9]. The two modes describing the dynamics of diffusion and self-bunching have been investigated numerically and theoretically, using a one-dimensional ($1d$) model system [5, 9] based on a mean field approximation and N-body simulation. In the mean-field approximation, the ion dynamics is modelled by the motion of a single charged test ion and a sphere of radius R uniformly filled with N identical ions moving in a model potential. Using this simple model, it was shown that in the self-bunching mode, as the number of ions in the sphere is increased, the motion of the test ion and the sphere are highly correlated, and the maximum distance between the sphere and the ion is bounded. On the other hand, in the dispersive mode, the bunch width was shown to increases much faster [5]. This simple model provided an insight about the minimum density of particles required for the self-bunching to occur [5, 8]. However, one-dimensional models are a crude approximation to the actual experimental conditions.

In this paper, we report about a two-dimensional particle-in-a-cell simulation (2DCylPIC) allowing for a detailed study of the ion dynamics in the cylindrical symmetric EIBT. Such simulation can mimic the experimen-

* Present address: Department of Physics, School of Advanced Sciences, Vellore Institute of Technology, Vellore, Tamil Nadu 632014, India
† Correspondence email address: oded.heber@weizmann.ac.il

tal conditions and reproduce the experimental data over a long storage time both in the dispersive and in the self-bunching modes. The simulation is used to investigate and reconcile various previous [5–8] and new experimental observations.

II. EXPERIMENTAL SETUP

The EIBT (see Figure 1) consists of two coaxial electrostatic mirrors, each composed of a stack of cylindrical electrodes. Depending on the configuration of the trap which is characterized by the potentials on six of these electrodes: V_p, V_1, V_2, V_3, V_4 and V_z, the EIBT can be operated in the diffusion or self-bunching mode of the trap. The schematic setup for the ion injection (SF_5^+ in the present study) in the EIBT is depicted in Figure 1.

The ions are produced in a pulsed (20 μs pulse duration) Even-Lavie supersonic expansion source [10]. The injected gas into the valve consist of SF_6 ($\sim$ 1 %) mixed with Argon as a carrier gas ($\sim$ 99 %) at a total pressure of 180 PSI. The mixture is supersonically expanded through the pulsed nozzle and is ionized by a electron pulse accelerated to an energy of about 200 eV, impacting the expanding gas $\sim$ 1 mm after the nozzle. The source is mounted on a high-voltage platform, which accelerates the ions to E_k = 4.2 keV, which then pass through a skimmer, an Einzel lens and a pair of orthogonal deflectors to be finally injected and trapped in the EIBT.

We use two different settings for the EIBT electrode potentials: In the diffusion mode these were $V_p = 5750$ V, $V_1 = 6500$ V, $V_2 = 4875$ V, $V_3 = 3250$ V, $V_4 = 1625$ V and V_z = 3400 V and for the self-bunching mode the values were $V_p = 4050$ V, $V_1 = 4700$ V, $V_2 = 4875$ V, $V_3 = 3250$ V, V_4 = 1625 V and V_z = 4050 V. All other electrodes were grounded. The ions were injected into the trap by lowering the left entrance electrode voltage V_p to $\sim$ 1600 V in the diffusion mode and to $\sim$ 2600 V in the self-bunching mode. The pressure in the trap was $\sim 3\times10^{-10}$ Torr and the average lifetime was on the order of 1000 ms [11]. Mass selection (in the present case for SF_5^+) was performed by adjusting the time delay between the voltage pulse operating the ion source nozzle and the entrance mirror. After each injection, the ions were trapped for about 800 ms. The time-dependent dynamics of the trapped ion bunch was recorded using the pickup electrode [11] (see Figure 1). The pickup electrode is slightly shifted from the center of the trap towards the exit mirror. The pickup is connected to the gate of a junction field transistor whose drain is fed to a charge sensitive amplifier. The amplified signal is recorded as a function of time with a 16 bit digital oscilloscope at a sampling rate of 10-50 MHz and, for each injection, subsequently stored in a computer and analyzed in real time. The time traces and the average time trace are analyzed directly and converted to the frequency domain via Fourier transform (FT). Depending on the exact electrode voltages, the half oscillation time (i.e., the time between each passing through the pickup electrode) was about 5.35 μs and 5.65 μs in the dispersive and self-bunching mode of the trap respectively.

III. 2D SIMULATIONS WITH ION-ION INTERACTION

The particle-in-cell (PIC) technique [12] has been widely used for many years for studying plasmas, gravitational systems, geodynamics, etc. In the present case, Poisson's equation is solved numerically on a computational grid, and the electric field at each grid point is obtained. The positions and velocities of simulation particles representing ions are then updated based on their location on the grid. Next, the new particle locations are used to update the charge density on the grid, at which point the electric field is recalculated. The simulation continues in this fashion until complete. The 3DCylPIC code [13] is a particle-in-cell code originally written to simulate ion trap and ion transport devices best modeled using a 3D cylindrical coordinate system. It has since been updated to support other 2D and 3D coordinate systems and is a natural choice in studying the ion dynamics in the EIBT. An overview of the code used here has been presented in [13], with additional applications demonstrated in [14], so only a summary and relevant new information will be provided here. First, the grid upon which the electric field is calculated is defined. This includes choosing the geometry, e.g., 2D cylindrical with azimuthal symmetry, 3D cartesian, etc., defining the physical size of the model space covered by the grid, and setting the resolution of the grid points. The particle storage objects are also initialized and provide a structure to store information such as position, velocity, mass, charge, etc., for each particle in the simulation. Next, any optional classes are initialized. These typically include routines to handle interactions with buffer gas or to handle boundary conditions inside the model space using the capacity matrix method [15]. Next, the boundary conditions are set to their initial values, usually associated with potentials applied to electrodes. At this point, the code enters a loop that is repeated in time steps of Δt, which is determined by the time scale of the physics involved (e.g., Radio Frequency (RF) period, particle velocities, mean free path, etc.). The general practice is to choose the largest value of Δt that doesn't significantly change the simulation results. In all the simulations described here a Δt=5 ns was used. The first step in the loop is distributing the charge associated with the particles in the simulation using the cloud-in-cell technique [16]. Particles can be created or lost at every time step, so the total amount of charge distributed on the grid can vary as the simulation progresses in time. Next, the electric potential is calculated on the grid. The simulations presented here use spectral methods, such as the one described in [16], as they are swift and accurate. Their major drawback is that one must use the capacity ma-

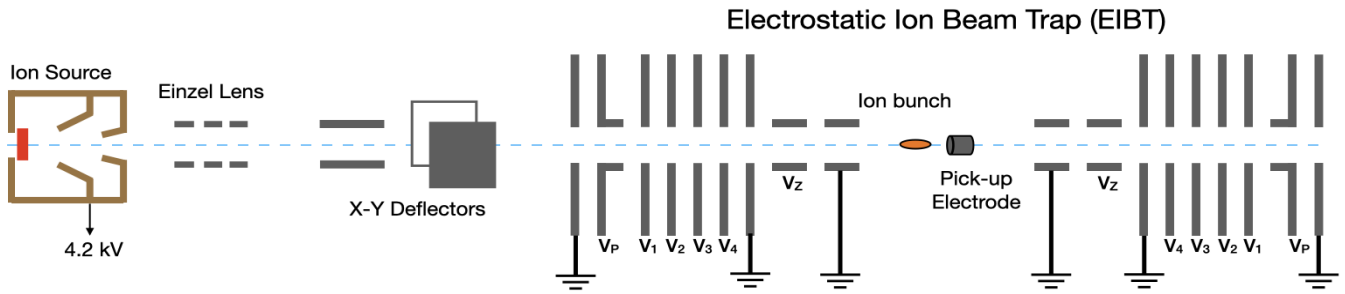

FIG. 1. Schematic view of the EIBT setup

trix method [13] to include boundary conditions inside the model space, and not just on the boundaries. After the potential has been calculated, the electric field at each grid point is determined by numerical differentiation. After the electric field has been calculated, the particle positions and velocities are updated using the leap-frog method [16]. In the final step, the time is incremented, boundary conditions are updated if necessary, and the loop repeats. This continues until an end condition is satisfied or the simulation is manually terminated.

The physical model space for these PIC simulations is a 2D axisymmetric (r-z) cylinder with a radius of $r_\circ = 8$ mm and length $z_\circ = 380$ mm with uniform grid spacings of dr = 0.05 mm and dz = 0.1 mm, respectively. $z_\circ = 380$ mm is the trap length. The radius of the model space was chosen to be equal to that of the minimum inner radius of the EIBT electrodes to avoid the need to use the capacity matrix method described above, which would increase the execution time of the simulation. The SIMION software package [17] was used to calculate the contribution to the total potential of each individual electrode on the boundary of the PIC model space, and was used to define the boundary conditions when calculating the total potential within the model space.

Since the pickup electrode is the primary experimental diagnostic tool of the ion dynamics in the EIBT, it is highly desirable to include it in the simulation. This is accomplished by designating some portion of the radial boundary of the model space as the pickup detector. Using a method similar to the one described in Appendix 6 of [18], applying Gauss' Law to the area specified as the pickup detector, the radial electric field is given by $E_r = \sigma/\epsilon_\circ$, where σ is the surface charge density and $\epsilon_\circ$ is the permittivity of free space. Each boundary point defined as part of the pickup detector defines an annular element with an area of $2\pi r_\circ dz$, so the total surface charge on a grid point, denoted by i, that comprises the pickup detector is $q_i = 2\pi r_\circ dz E_{r,i}\epsilon_\circ$. By summing over all q_i of the pickup detector, the total induced charge is calculated which exhibits periodic peaks as the ion bunch passes through the pickup detector. A typical time trace of the pickup signal as it passes through the pickup detector is shown from the experiment (top) and simulation (bottom) in Figure 2.

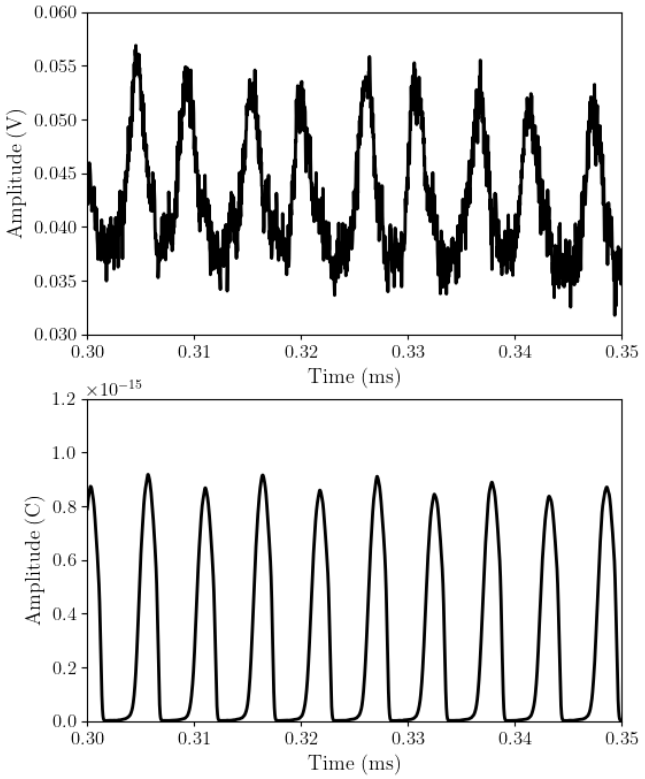

FIG. 2. Example of the time trace of the pickup signal as recorded in the experiment (top), where the pickup electrode is located slightly shifted towards the exit electrodes and simulation (bottom), where the pickup electrode is located exactly at the center of the trap from 0.3 ms to 0.35 ms. Time zero in the simulation and experiment are not equal. Since in the experiment the injection is included while in the simulation it is from the center of the trap.

A. Simulation operation and initial ion distribution

The present simulations were carried out, both in the dispersive and the self-bunching modes in a setting that represents as closely as possible the experimental setup. However, the injection process itself was not simulated, and the ion bunch was initially located at the center of the trap with an initial bunch width of 30 mm (corresponding to a bunch width (FWHM) of 0.9 μs), a radius of about 4 mm in the dispersive mode and 2 mm in the self-bunching mode of the trap, a kinetic energy of 4.2 keV and an initial spread of 3 eV, that closely matches the experimental conditions. For some specific cases, to match the initial experimental conditions, the initial width has been varied accordingly. No attempt was made to study the effect of beam emittance in this work, as it very much depends on the experimental conditions upstream of the trap, and is not an intrinsic property of the trap. To analyze the pickup and simulation data, a windowed thresholding method was created and used to extract the FWHM of each peak. The details of the data analysis method are given in Appendix A.

IV. RESULTS AND DISCUSSION

A. Dispersive mode

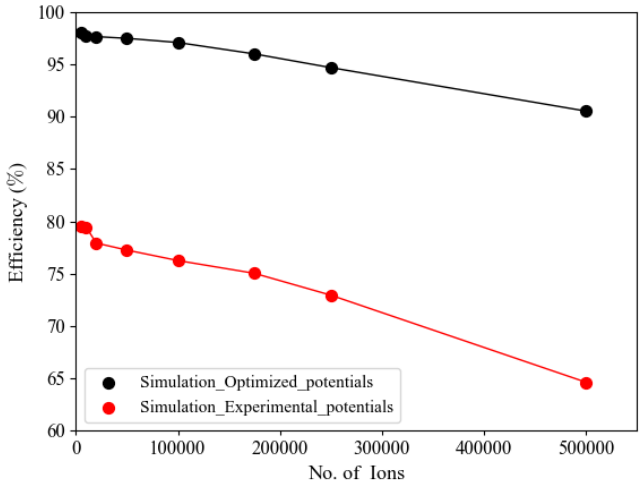

FIG. 3. Simulated trapping efficiency ε as a function of the number of injected ions in the diffusion mode of the trap with space charge for experimental (red dots) and optimized potentials (black dots). The slip factors for the experimental and optimized potentials are -0.645 ± 0.006 and -0.639 ± 0.003 respectively. The lines are drawn to guide the eyes

While the trap has been proven to be stable under the conditions defined in [19], which are similar to an optical resonator, these conditions do not include the effects of space charge. To provide an estimate for the loss of particles in the trap due to space charge, a simulation was carried out with an increasing number of particles (having 0.9 μs as initial bunch width) for a trapping time of 10 ms. The simulation was first performed using a set of electrode potentials identical to the experimental ones. These potentials were then varied to find whether the trapping efficiency could be improved. In Figure 3, we plot the trapping efficiency (ε), which we define as the percentage of ions with stable trajectory after a storage time of 10 ms, as a function of the initial number of ions N_0 injected in the trap for both the experimental set of electrode potentials (red) as well as for the optimized one (black: We found $V_1 = 5680$ V and $V_z = 3100$ V, all other potentials being identical to the experimental ones). Using the potential as in the experiment, for a very small amount of particles ε is about 79%. Increasing the number of ions in the trap results, as expected, in a decrease of the trapping efficiency, in the range of 65% for about half a million ions. However with the optimized mirror potentials, the efficiency of trapping could be increased by more than 15% to ε=98 % for a small number of particles to about 90% for half a million ions. Such optimized potentials are important for experiment requiring long trapping time. Overall, these results show that while space charge has, as expected, an effect on the trapping efficiency in the dispersive mode, it is not a major one. No attempt was made to simulate the initial emittance of the ion beam, which is most likely the reason for the initial offset for the trapping efficiency.

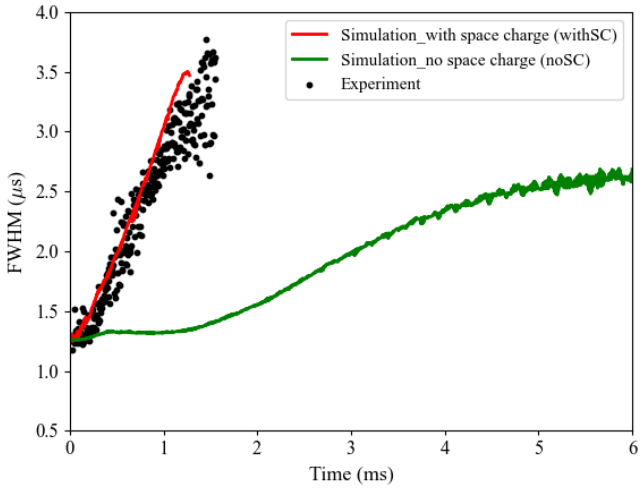

FIG. 4. Time dependent FWHM for a stored ion bunch with 175,000 ions in the dispersive mode. The black dots are the results of the experiments while the red and green lines are the simulation results with and without space charge, respectively

A very important question about the dynamics of ion bunches in the trap is the time evolution of a bunch. Understanding such evolution is critical, for example, while trying to use the EIBT as a long time of flight mass spec-

trometer. While a simple model can be used to understand such dynamics without space charge (but including kinetic energy spread), including this effect requires a more detailed calculation. For this purpose, we simulated and measured (under identical conditions) the time dependent FWHM of a stored bunch width injected in the trap with various initial number of ions. Figure 4 illustrates the measured FWHM (black dots) for a 4.2 keV SF_5^+ ions injected with an initial FWHM of about 1.24 μs (42 mm). The data shows the rapid growth of the bunch size, filling up the trap in about 1.6 ms of storage time. The simulation (red line) is able to reproduce the experimental data assuming that the initial bunch includes about 175,000 ions. To visualize the importance of the space charge contribution to the bunch width broadening, a similar simulation was carried out without space charge (green line), showing, as expected, a much slower widening of the bunch, mostly due to the initial energy distribution and the slightly different length of trajectories allowed in the trap. In the case of no-space charge, for each time step the field is calculated using the charges of the ions just to get the induced signal on the detector. Then again, the field is calculated without using the ions charge, which is used to move the ions. This enables to get the induced signal on the pickup detector for no space charge case and the FWHM for comparing with the space charge case for consistency. Simulations performed with the optimized potential yield similar results.

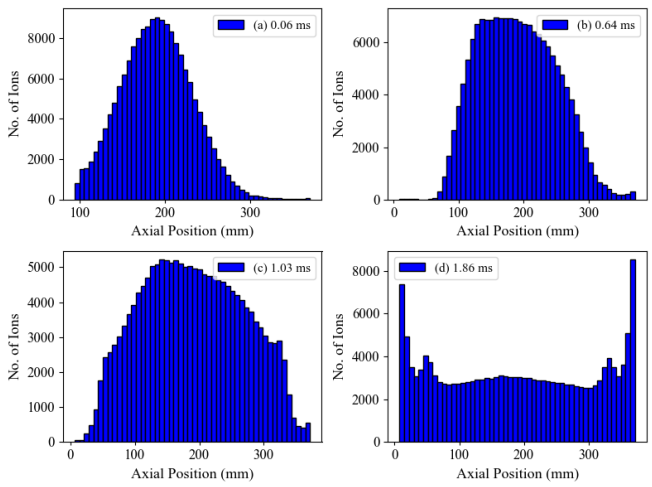

FIG. 5. Axial distribution of the ions with time in the dispersive mode of the trap with space charge for 175,000 ions

As an additional illustration of the bunch behavior, Figure 5 shows the simulated evolution of the axial distribution of the ions with time in the dispersive mode of the trap with space charge effect. The axial distributions of ions are recorded every time the mean axial position of all the ions crosses the center of the trap. The initial axial standard deviation is set to be identical to the experimental values used in the simulation (bunch width=42 mm or 1.24 μs). Figure 5(a) shows the initial distribution at the beginning of the simulation, Figure 5(b) and Figure 5(c) show a snapshot after 0.64 ms and 1.03 ms of storage time, respectively. Figure 5(d) shows the steady state distribution (here after about 1.86 ms), once the bunch is fully spread in the trap. The high density of ions at the edges is due to the much slower velocity of the ions within the mirror areas.

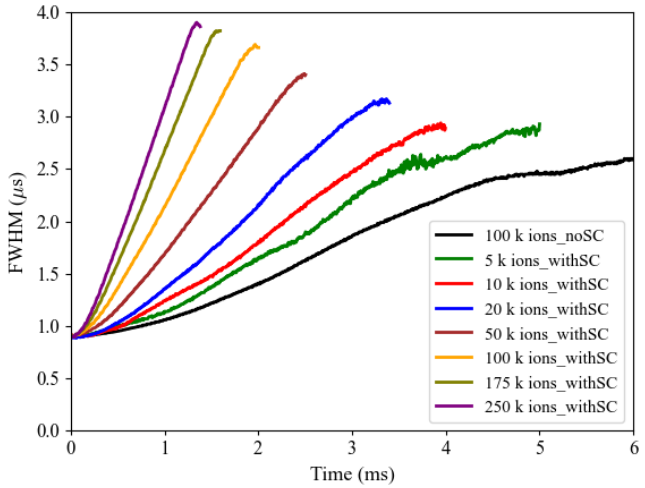

FIG. 6. Simulated time dependent FWHM of the stored bunch width (initial width = 0.9 μs) as a function of the number of injected ions in the dispersive mode. For comparison, the black curve is calculated without space charge case with a total of 100,000 ions.

Given the importance of the space charge effect on the bunch width, we simulated the bunch time development as a function of the number of ions. Figure 6 shows the evolution of the FWHM (initial width = 0.9 μs) of the bunch for varying number of ions from 5,000 to 250,000 ions. For comparison, the FWHM for no-space charge case is also included (black line) for 100,000 ions. The results, shown in Figure 6, demonstrate the strong space charge effect on the time-dependent FWHM of the bunch in the dispersive mode of the trap. The data is shown for the maximal trapping time for which a fit still faithfully represents the ion distribution within the bunch. Such results are quantitatively important when using the trap in the dispersive mode, as a very long time-of-flight mass spectrometer [20]. Indeed, one could think of the EIBT as an extremely long time-of-flight mass-spectrometer (TOFMS), but the results shown here demonstrated the importance of the space charge effect on the bunch widening. This effect is much stronger in the EIBT than in a field-free TOFMS, due to the relatively high density of ions at the turning points in the mirrors. On the other hand, since in a typical TOFMS, the time-of-flight is only of the order of few to tens of microseconds, the EIBT can be used to increase this time-of-flight by at least an order of magnitude, especially with low ion density, without

increasing the bunch size, before extracting the trapped ion and measure their time of arrival on a typical micro-channel plate, similar to a standard TOFMS. Example of such methods, for a very low ion density, have already been demonstrated in Ref [21].

B. Self-bunching mode

Similar to the dispersive section IV A, the trap efficiency ε was investigated in the self-bunching mode. Figure 7 presents the results as a function of the number of injected ions N_0 for 100 ms in the self-bunching mode of the trap with space charge interaction for an initial bunch of 0.9 μs. It is evident from these results that the efficiency decreases quicker than for the dispersive mode, as the number of ions is increased from 5,000 to 250,000 ions. The trapping efficiency for 1,000 and 250,000 ions after 100 ms of trapping are $\sim$ 85 % and $\sim$ 9 % respectively. This rapid decrease in efficiency for large number of ions is the direct result of the self-bunching phenomena which increases the space charge effect by keeping the ions bunched for very long trapping time, hence the need to compute the efficiency over a longer storage time (100 ms) than for the dispersive mode (10 ms), as shown in Figure 3. These results demonstrate that while the EIBT can be used in both modes of operation, the contribution of the space charge to the trapping efficiency (and hence the lifetime) is more critical in the self bunching mode than in the dispersive mode. On the other hand, it shows (and will be discussed in more details below) that even a small amount of ions is enough to produce self bunching.

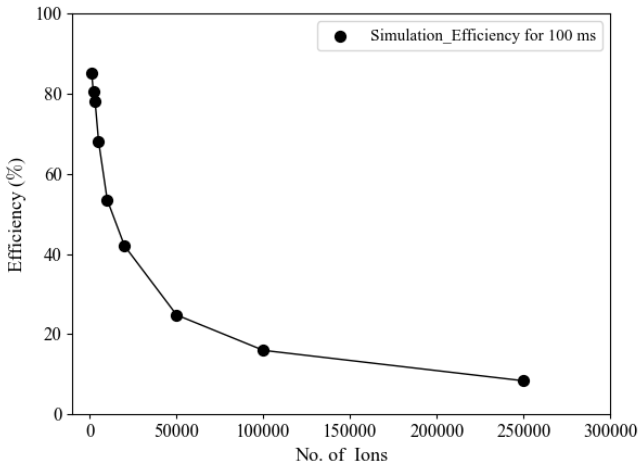

FIG. 7. Efficiency (ε) vs number of ions in the self-bunching mode of the trap with space charge for 100 ms. The line is drawn to guide the eye

To demonstrate the self-bunching effect, the FWHM of a simulated ion bunch time evolution is shown in Figure 8 as red (with space charge) and green (without space charges) lines. The experimental results are shown as black dots. The simulation is performed for 50000 ions with an initial FWHM of 1.8 μs to match the experimental conditions, for a total storage time of 100 ms. As can be seen in Figure 8(a), in this configuration, the FWHM of the ion bunch rapidly decreases to about 0.75 μs. Additional changes in the FWHM can be seen in the data at later storage time, most likely due to the capture and release of ions which are not part of the bunch due to their initial specific trajectories and/or energies. These oscillations persist until around 20 ms, after which the FWHM remains more or less constant as time evolves, as shown in Figure 8(b). The simulated data with space charge interactions (red line) has a similar behavior, within the uncertainty of the data. The simulation data for no space charge (green line) initially shows a decrease in the FWHM, which is likely due to the shallow potential gradient, before it starts to increase again similar to the diffusion mode and eventually filling up the trap after a storage time of about 20 ms. These simulation results clearly demonstrate that the self bunching effect is due to the combined effect of the slip factor η (see Eq.1) being positive and the space charge effect. These two effects acting together create a situation where (1) the faster ions in the bunch have a longer oscillation time than the slow ones because they spend more times in the mirrors regions of the trap, hence these ions are located at the trailing side of the bunch while (2) in this situation, the Coulomb repulsive forces among the ions tend to slow down the fast ions and speed up the slow ions. This peculiar effect has been shown to be useful for mass measurement using Fourier Transform of the pick up signal over long storage time. The fact that it can be reproduced using this simulation opens the door for further calculations where the impact on mass resolution and mass separation due to space charge can be studied in more detail (see Section IV C below).

Similarly to Figure 5, the time evolution of the axial distribution of ions in the self-bunching mode with space charge is shown in Figure 9. Figure 9(a) shows the distribution width after 0.06 ms of storage, namely at the beginning of the simulation. Then in Figure 9(b), 9(c) and 9(d), the axial distribution is presented for all trapped ions at 23.36, 53.44 and 99.56 ms, respectively. The narrowing of the bunch width, as shown in Figure 8, is clearly seen. The self-bunching continues for more than 100 ms of storage time, and is only limited by the maximum simulation time and the requirement for minimum ion density (see below). It is also clear from these results that while an injected ion bunch can survive in the trap for quite a long storage time, more and more ions are slowly lost from the bunch (albeit not from the trap), filling up the trap and losing synchronization with the initial bunch.

In order to better characterize this effect and find its dependence on the ion density, the simulated, time-dependent FWHM for various number of ions (from 5,000 to 100,000) in the self-bunching mode is shown both in Figure 10(a) (for up to 5 ms of storage time) and 10(b)

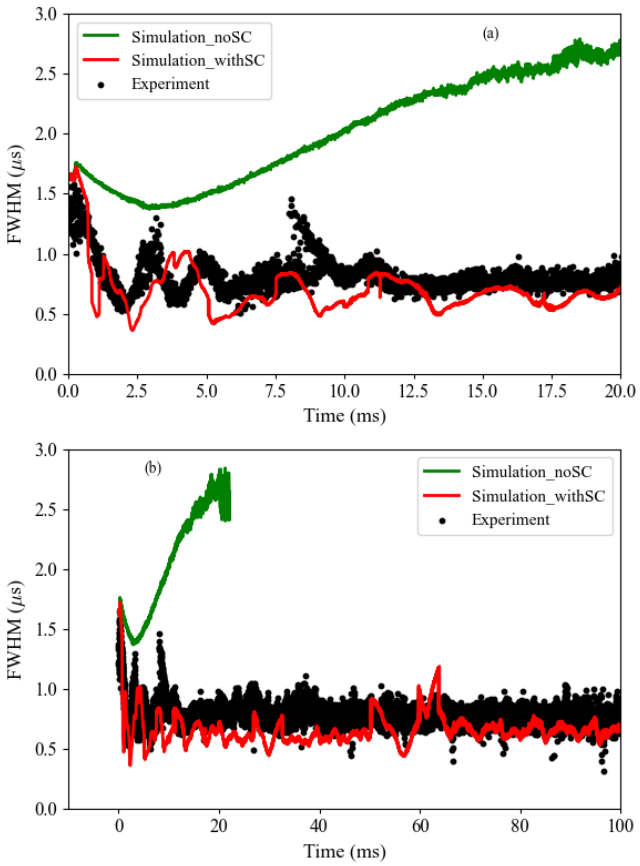

FIG. 8. Comparison between the time dependent simulated (lines) and the measured (black dots) FWHM for a trapped ion bunch in the self-bunching mode (a) 20 ms and (b) 100 ms. The simulation is performed for 50,000 ions. The red and green lines are the result of the simulation with and without space charge, respectively

(for up to 100 ms of storage time). The case for no space charge for 100,000 ions is also included in the figures for comparison (black line). As in Figure 8, a fast decrease of the FWHM is observed at the beginning for all cases, with faster narrowing being observed for higher charge density. After 10 ms the FWHM seems to stabilize (see Figure 10(b)) to a constant value which depends on the number of ions: The higher the number of ions, the larger the stable bunch is. Here for 100,000 ions with space charge a complex oscillating behavior is seen that may be due to the internal bunch dynamics and interaction with residual ions. For the no space charge case, the FWHM shows a slow increase and fills the trap within 25 ms, as in Figure 8. However, the initial decrease of the bunch width as seen in Figure 8 for the initial bunch of 1.6 μs is not seen when the simulation is performed for the ion bunch starting with a smaller width of 0.9 μs (see Figure 10). This is further investigated by varying the initial width with no space charge in the self-bunching mode and the results are shown in Figure 11.

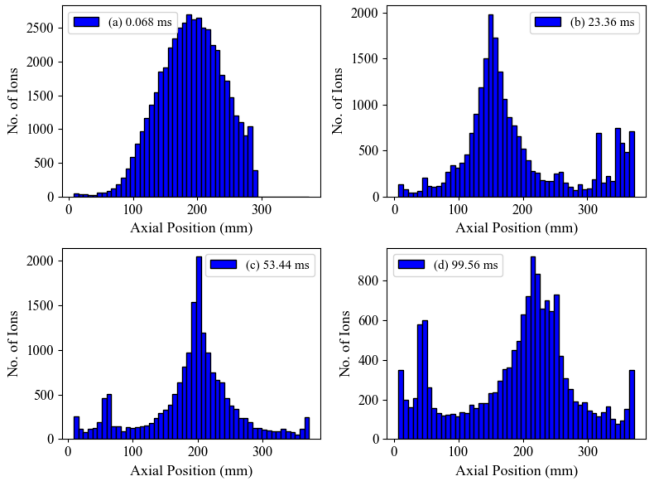

FIG. 9. Axial distribution of the ions at different time stamp in the self-bunching mode of the trap with space charge effect for 50,000 ions

Figure 11 shows simulated data for varying initial FWHM for 50,000 and 100,000 ions in the self-bunching mode of the trap without space charge interactions for 10 ms. It is been seen that for larger initial FWHM, there is a dip in the FWHM initially for the simulation starting with the initial bunch width of 1.63 and 2.08 μs till about 5 ms, which subsequently rises after that. The dip in the FWHM at the start is more pronounced for larger initial width and it goes down systematically with smaller initial bunch widths and we no longer see a dip at the beginning for the cases of 0.9 and 0.34 μs. Since there is no space charge interaction involved in these calculations, the effect is purely of the shallow potential gradient of the self-bunching mode, that affects the dynamics of ion bunches as it evolves with time and the effect is more dramatic for larger initial widths. The simulated data for 100,000 ions is also included for two cases of 0.9 and 1.63 μs initial bunch widths and the results are similar to that of 50,000 ions cases as expected since there are no space charge interaction involved in these cases.

Given that the space charge is the main factor affecting the self-bunching, we have studied the low density regime in greater detail. Of course, the minimum density of ions needed to achieve self-bunching will depend on additional parameters, such as the specific beam energy, the initial bunch size, or the exact configuration of the trap. However, one factor which is clearly working against the self-bunching is the initial beam energy spread. For this purpose, we have carried out a series of simulation focused on low ion density for 1,000, 2,000, 3,000 and 4,000 ions with a fixed initial width of 0.9 μs and for an initial energy spread of 3 eV and 5 eV. The results are shown in Figure 12(a) and (b) for an initial energy spread of 3 eV and 5 eV respectively. The self-bunching effect is observed in all cases, for an initial energy spread of 3 eV (Figure 12(a)). However, for

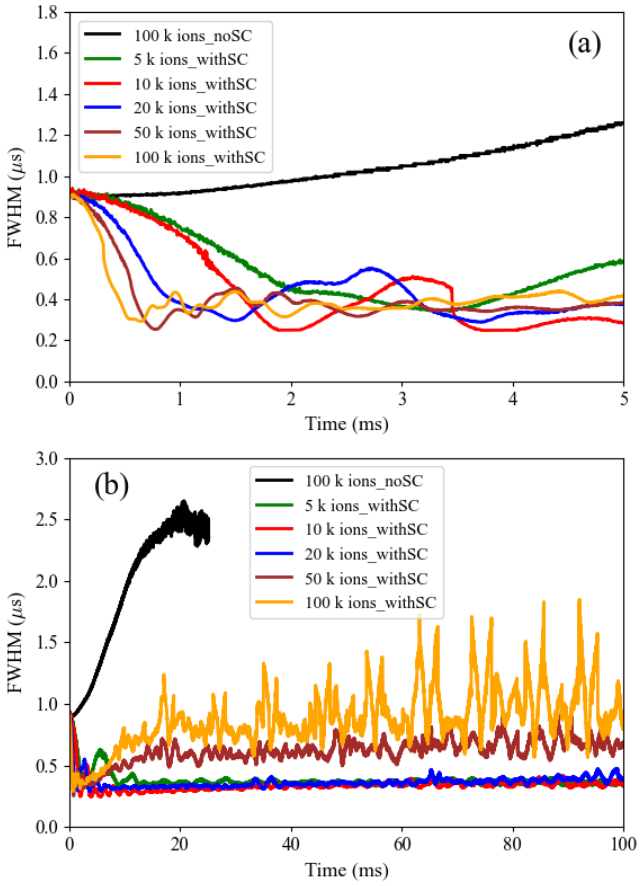

FIG. 10. FWHM calculated for varying numbers of ions used in the simulation starting from 5,000, 10,000, 20,000, 50,000 and 100,000 ions with space charge effect for the initial width of 0.9 μs; a simulation data without space charge effect for 100,000 ions is also included for comparison; (a) shows the simulation results for the first 5 ms and (b) shows the results for the whole 100 ms.

an initial energy spread of 5 eV (Figure 12(b)), the data clearly shows that 1,000 ions are not enough to stabilize the bunch which rapidly grows in size (black line). As expected, these results clearly show that a minimum number of ions are needed to sustain the self-bunching effect, and that this low limit depends on the energy distribution of the incoming ion beam. However, this low limit is surprisingly small (of the order of a thousand ions in a 0.9 μs bunch) for a beam energy width of about $\Delta E_k/E_k = 10^{-3}$. While more studies are needed to characterize this limit in a systematic way, including the mass dependence, these numbers suggest that such a system could be of use in practical mass spectrometry system, where such energy resolution and number of ions are typical. We investigate this aspect in the next section, using the simulation.

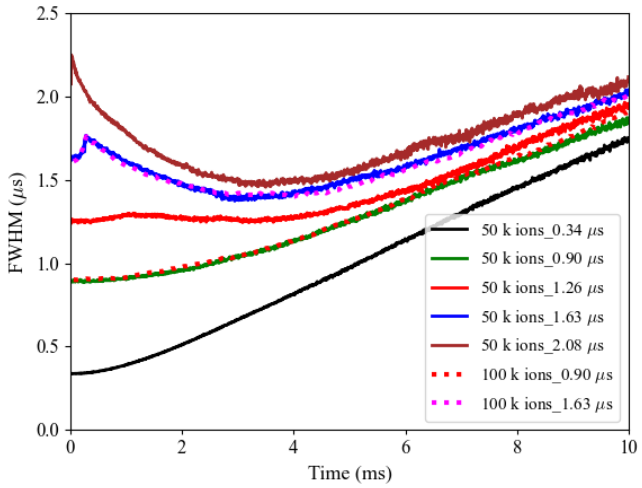

FIG. 11. FWHM calculated for 50,000 ions (self-bunching mode of the trap with no space charge) for various initial width of 0.34, 0.90, 1.26, 1.63 and 2.08 μs as well as for 100,000 ions, for 0.90 and 1.63 μs initial bunch as a function of trapping time.

C. Mass spectrometry applications

One of the earliest type of mass spectrometers is the time-of-flight mass spectrometer (TOFMS) [22, 23], whose resolution depends largely on the length of the flight tube and the dispersion due to velocity spread. TOFMS mass resolution and detection sensitivity decreases with increasing mass, and they can reach mass resolving power of 10^3-10^4 with relatively good efficiency. Another type of mass spectrometer with excellent mass resolving power and high efficiencies, even for larger mass, is the Fourier-transform ion cyclotron resonance mass spectrometer (FTICR-MS)[24, 25]. FTICR-MS can reach the mass resolving power of up to 10^5 with high efficiency, but requires superconducting magnets with fields higher than 10 T for mass spectrometry studies of larger bio-molecules and nano-particles. The current generation of multi-reflection time-of-flight mass spectrometer (MR-TOF-MS) can achieve mass resolutions of 10^6 and relative mass precision up to 10^{-8} [26], which is adequate to provide precise information on nuclear binding energies and unambiguous species identification. MR-TOF-MSs are fast, efficient, high-precision instruments that have been steadily improving in performance and have proven to be versatile beam diagnosis and optimization tools [27]. Other devices, such as the Orbitrap, can also be used for similar purposes [28].

One of the questions often asked about the EIBT is its possible application as a mass spectrometer. In other words, could the EIBT in the self-bunching mode separate ions of various masses (with identical kinetic energy)? As the trap is purely electrostatic, the oscillation time of the ions depends on the mass-to-charge ratio

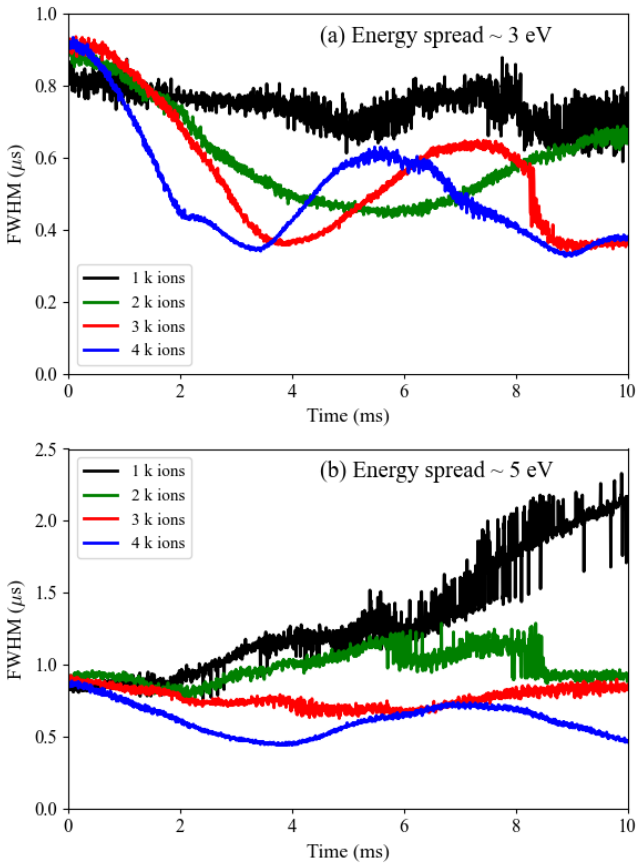

FIG. 12. FWHM calculated for varying numbers of ions (1,000, 2,000, 3,000 and 4,000 ions) for the same initial width of 0.9 μs and different energy spread ΔE_k of (a) 3 eV and (b) 5 eV in self bunching mode.

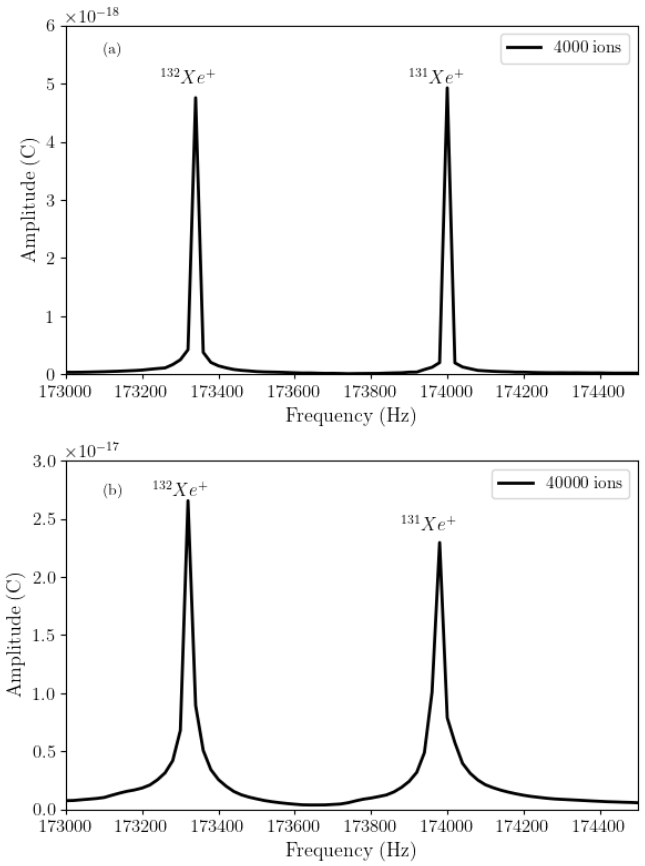

FIG. 13. Fourier transform of the pickup signal (from simulation) for the two Xe isotopes (131 and 132) trapped together in the self-bunching mode for 50 ms for (a) 4,000 ions and (b) 40,000 ions (bottom)

given as $T = 1/f \propto \sqrt{(m/q)}$, where T is the oscillation time, f is the frequency of oscillation, m and q are the mass and charge of ion, respectively. The EIBT has already been shown to act a mass spectrometer [20, 29] with high resolving power of the order of (10^5-10^6) experimentally. On the other hand, coalescence of bunches of ions of similar mass has been observed experimentally in the self-bunching mode [30]. It was also shown that the coalescence effect appears when the number of ions in the close-mass peaks exceeds a certain threshold using a 1D model and the Coulomb interaction between ions of similar mass has a resonant nature [31]. However, no systematic (simulation) study has been performed to understand the possible effect of bunch coalescence in the case where two (or more) different type of ions, with different masses, are being trapped and self bunched.

An initial simulation test was performed by trapping two singly charged isotopes of Xe, namely, $^{131}Xe^+$ and $^{132}Xe^+$ for 50 ms in the self-bunching mode with an initial FWHM of 1 μs and an energy spread of 3 eV. Figure 13 (a) and (b) show the Fourier transform (second harmonic) of the pickup signal obtained from the trapping of two Xe isotopes, for 4,000 and 40,000 ions, respectively. In both cases, the two peaks are clearly separated. The FWHM of the peaks shown in Figure 13 (a) are about 20 $\pm$ 0.50 Hz, which corresponds to $\delta m/m = 2\delta f/f \sim 2.3 \times 10^{-4}$, while in Figure 13 (b) the FWHM of the peaks are broadened a bit due to space charge interactions and is about 27 $\pm$ 2 Hz, corresponding to $\delta m/m = 2\delta f/f \sim 3.1 \times 10^{-4}$. The fit is using the tails of the distribution, resulting in a better accuracy than the binning. The resolution of the peaks are only limited by the trapping time and much higher resolution is possible. From a simple calibration procedure, the expected frequency difference Δf between these peaks representing the two masses of $^{131}Xe^+$ and $^{132}Xe^+$ should be about 660.34 Hz. The corresponding frequency difference from the simulation with 4,000 and 40,000 ions is about 660.11 Hz and 658 Hz, respectively. These results show that for relatively low mass, and for low bunch density, the EIBT, in the self bunching mode, is able to be operate as a precise mass spectrometer. On the other hand, the effect of higher ion density is also clearly observed as the frequency difference decreases with the increase in

ion's density.

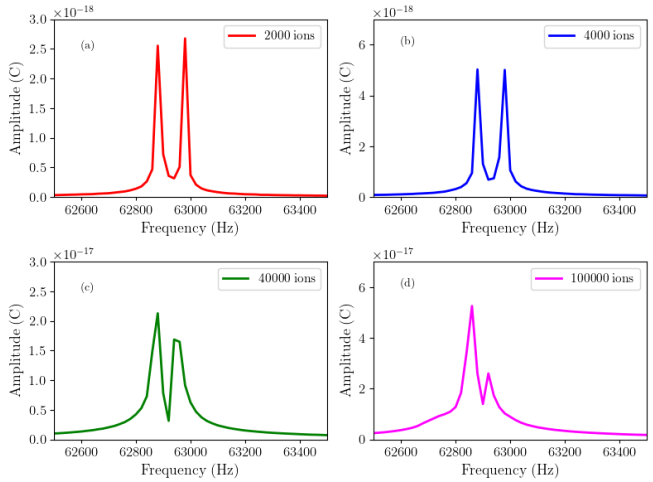

FIG. 14. Fourier transform of the pickup signal (from simulation) for the two masses (1,000 and 1,003) trapped together in the self-bunching mode of the trap (a) 2,000 ions; (b) 4,000 ions; (c) 40,000 ions and (d) 100,000 ions

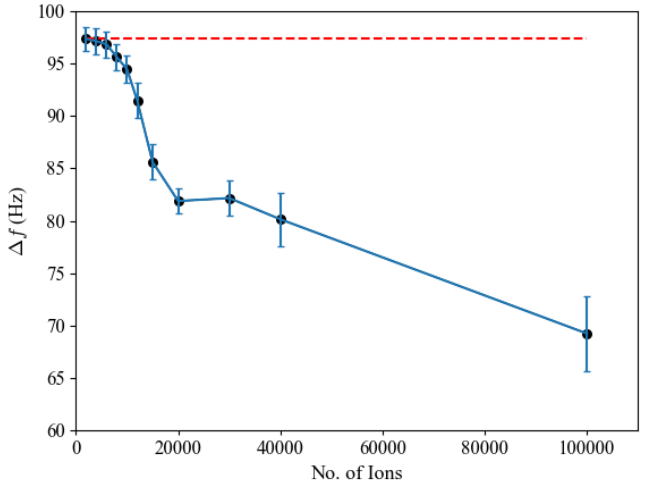

FIG. 15. Simulated frequency difference (Δf) between the nearby masses 1,000 and 1,003 as a function of number of ions in self bunching mode. The error bars are calculated from the standard error in the mean value of the Gaussian fit. The dashed line is the expected frequency difference obtained by trapping each mass separately. The line is drawn to guide the eyes.

To gain further insight into the effect of peak coalescence for higher mass, we run a series of simulations with masses of 1,000 and 1,003 for different number of ions. The simulation was performed as a function of the number of ions in the bunches (identical for both masses). Figure 14 shows the Fourier transform (second harmonic) of the pickup signal for the four cases of 2,000, 4,000, 40,000 and 100,000 ions. The results show that for small number of particles (2,000 and 4,000), the peaks are well resolved with a FWHM of about 22 Hz, which corresponds to $\delta m/m = 2\delta f/f \sim 7\times10^{-4}$ and the frequency separation is about 97.34 Hz, while for 40,000 and 100,000 the coalescence effect is clearly seen.

In order to quantify this, we show in Figure 15 the frequency difference Δf as a function of the number of ions in the self bunching mode for a storage time of 50 ms. The coalescence effect is clearly apparent starting from 15,000 ions, but relatively minor for less ions, and is asymptotically approaching the value expected (shown as a dashed line) if these two ions would have been stored separately, as tested by running the simulation for each mass separately.

These results show that while peak coalescence is a major concern for large number of ions, it can be minimized by trapping relatively small number of ions. While more simulations are needed to fully characterize this effect for different range of masses, energies and slip factors the simulation developed here is a first step toward understanding this phenomena, and the limitation it imposes on the use of a EIBT as a mass spectrometer.

V. SUMMARY

In this work, we have developed a particle-in-cell simulation technique to study the dynamics of ions trapped in an EIBT both in the dispersive and in the self-bunching mode of the trap. The simulation results have been compared with experimental data, and overall a good agreement is found. The main aspect of this study has been to understand the role of the ion-ion interaction in the dynamics of ions in the trap. In the dispersive mode, we have found that the ion-ion interaction leads to faster dispersion of the ion bunches; while in the self-bunching mode it leads to the preservation of the ion bunches for more than 100 ms, limited by the time of the simulation or minimum ion density criteria. The simulation also enables characterization of the peak coalescence in a more quantitative way, demonstrating the value of the EIBT as a high resolution/separation mass spectrometer that, when operated in the self bunching mode with low ion density, allows for self bunching and avoids coalescence. The study of time dependent ion dynamics using external RF and chirp pulse to understand the auto resonance cooling of ions [6] is under progress.

VI. ACKNOWLEDGEMENTS

D.G. acknowledges financial support from a Dean of Faculty Fellowship of the Weizmann Institute of Science. R.R. and C.N. acknowledge support from the U.S. National Science Foundation through Grant Nos. PHY-

1565546 and PHY-2111185. Computational resources and services were provided by the Institute for Cyber-Enabled Research at Michigan State University. This research was supported by the ISRAEL SCIENCE FOUNDATION (grant No. 1214/17).

Appendix A: Data Analysis

To analyze the signal from the pickup electrode in both experimental and simulation data, a windowed thresholding method was developed and used to extract the full width at half maximum (FWHM) of each peak. This choice was made because both the simulated ion bunches and the ion bunches detected by the pickup electrode were often asymmetric and varied in shape, with no known analytical form. This makes extracting FWHM information from Gaussian or Lorentzian fits to the data unviable.

1. Windowing

To reduce the influence of a non-constant DC baseline between peaks, it is necessary to chop the data into windows containing only a single peak. An initial number of data points is defined as the window width, with a few additional parameters controlling how the peak finding algorithm responds in the case of no peak found or multiple peaks found. In the case of no peak found, the window width increases by a given number of data points up to a pre-defined maximum width. In the case of multiple peaks found, the window width decreases by a given number of data points down to a pre-defined minimum width. In the case that the maximum or minimum window width has been reached but a single peak was not found, the window is advanced a given number of data points until a peak is located. In this way, the peak finding algorithm dynamically controls the window width and translates it along the time axis to capture individual peaks representing ion bunches. This helps to linearize the baseline, which is not flat and exhibits significant undershoot, by constraining it close to the peak.

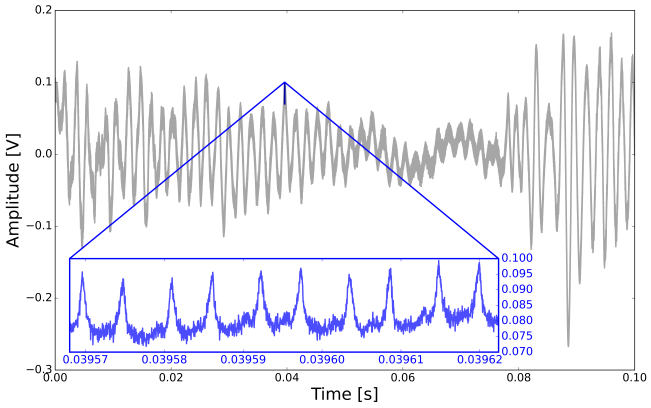

FIG. 16. Raw experimental pickup data, used for the analysis shown in Figure 8, which illustrates the variation in the baseline. The data were acquired over duration of 100 ms and contain over 17,000 ion peaks. The zoom inset makes a small subset of the peaks generated by the ions visible on top of the baseline.

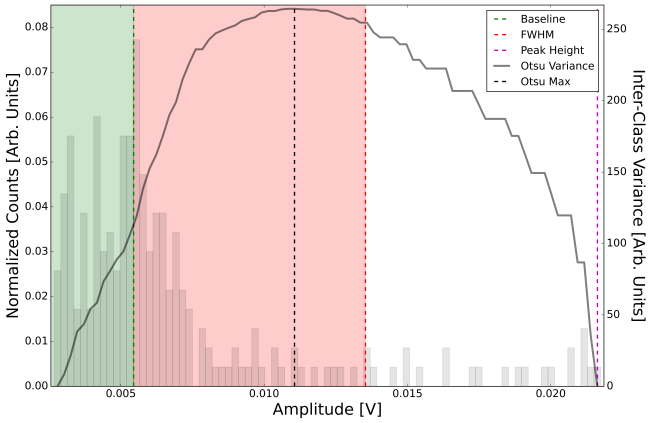

FIG. 17. Binned data from the seventh peak shown in the inset from Figure 16. The green shaded area contains data below the baseline. The red shaded area contains the data between the baseline and the half maximum amplitude value. The solid line is the calculated Otsu variance, and the black vertical dotted line marks the point of maximum variance and the division point between the left and right sections. The peak height is defined as the the last bin in the histogram.

2. Thresholding

The method described in this supplement is used both to locate peaks and extract the FWHM information.

First, the data in the window is lightly smoothed using a Savitzky-Golay filter [32] with a given polynomial order and window size. This filter type can greatly reduce noise with minimal peak distortion. The smoothed data is then placed into a histogram.

The number of histogram bins chosen needs to be large enough for the chosen threshold, Otsu's Method [33], to work well. For Otsu's Method, it is important for the histogram to be a bimodal distribution so the variance between the two modes can be maximized. In practice, the baseline is found in one of the modes and the top of the peak is found in the other.

To create enough bins such that the resulting histogram is bimodal, but not so many bins that the bimodal structure is lost, the number of bins N is calculated using the number of data points n by multiplying a modification of Sturges' formula [34] with the standard Square-root formula:

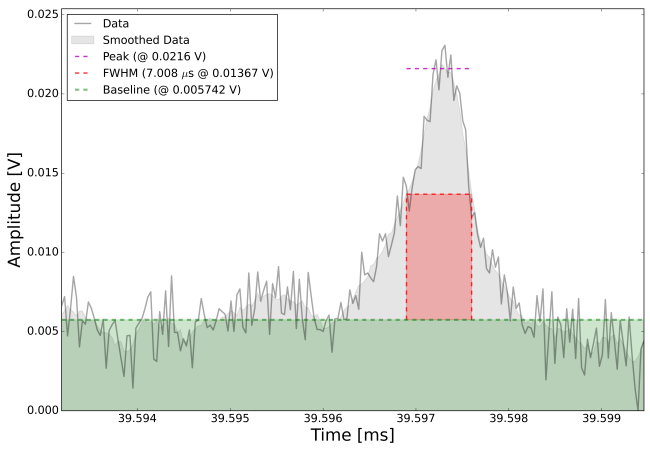

FIG. 18. The raw and smoothed data from the seventh peak shown in the inset from Figure 16. The adaptive windowing algorithm has clearly isolated a single peak, smoothed the data, applied the threshold, and extracted the FWHM. Note that the peak would be poorly approximated by a Gaussian or Lorentzian fit.

$$N = \ln n * \sqrt{n} \tag{A1}$$

This formula was chosen after systematically trying most of the well known binning methods and combinations thereof.

After binning, Otsu's Method is applied to divide the histogram at the point of maximum variance into left and right sections. An example of this process is shown in Figure 17.

To the left of the maximum variance, the signal baseline is taken as either the mean or median of the data in that section, whichever is smaller. The green shaded region indicates the detected baseline level. The maximum height of the signal is defined as the last bin in the histogram. The distance between the baseline and the maximum height is taken to be the full height, from which the half maximum height is calculated. The red shaded area contains the signal values that fall between the baseline and half maximum height.

3. FWHM

Once the half maximum height is found, the smoothed signal data is analyzed by an algorithm that applies certain constraints to ensure only a single peak is found in the window.

First, the half maximum height is applied as a threshold. Only data above this threshold will be considered a potential peak. Then, the left and right locations where each peak intersects the half maximum height are calculated. If a potential peak's width is above a predefined value and the peak is not too close to the left or right side of the windowed region, the peak is analyzed further.

If the data are noisy, narrow peaks sufficiently close to one another are not interpreted as individual peaks, but instead are merged into a single peak. This merging behavior is configurable.

The list of peaks found in the window is then returned to the main windowing algorithm for processing. If exactly one peak is found, then the smoothed signal data are interpolated around the half maximum height to extract the FWHM. Otherwise, the window is adjusted according to the procedure in A 1.

The result of the analysis of this single peak is shown in Figure 18.

[1] D. Zajfman, O. Heber, L. Vejby-Christensen, I. Ben-Itzhak, M. Rappaport, R. Fishman, and M. Dahan, Phys. Rev. A **55**, R1577 (1997).

[2] M. Dahan, R. Fishman, O. Heber, M. Rappaport, N. Altstein, D. Zajfman, and W. J. van der Zande, Review of Scientific Instruments **69**, 76 (1998), https://doi.org/10.1063/1.1148481.

[3] L. H. Andersen, O. Heber, and D. Zajfman, Journal of Physics B: Atomic, Molecular and Optical Physics **37**, R57 (2004).

[4] A. Yariv, *Quantum electronics*, 3rd ed. (Wiley, New York, 1989).

[5] H. B. Pedersen, D. Strasser, B. Amarant, O. Heber, M. L. Rappaport, and D. Zajfman, Phys. Rev. A **65**, 042704 (2002).

[6] R. K. Gangwar, K. Saha, O. Heber, M. L. Rappaport, and D. Zajfman, Phys. Rev. Lett. **119**, 103202 (2017).

[7] H. B. Pedersen, D. Strasser, S. Ring, O. Heber, M. L. Rappaport, Y. Rudich, I. Sagi, and D. Zajfman, Phys. Rev. Lett. **87**, 055001 (2001).

[8] M. W. Froese, M. Lange, S. Menk, M. Grieser, O. Heber, F. Laux, R. Repnow, T. Sieber, Y. Toker, R. von Hahn, A. Wolf, and K. Blaum, New Journal of Physics **14**, 073010 (2012).

[9] D. Strasser, T. Geyer, H. B. Pedersen, O. Heber, S. Goldberg, B. Amarant, A. Diner, Y. Rudich, I. Sagi, M. Rappaport, D. J. Tannor, and D. Zajfman, Phys. Rev. Lett. **89**, 283204 (2002).

[10] U. Even, J. Jortner, D. Noy, N. Lavie, and C. Cossart-Magos, The Journal of Chemical Physics **112**, 8068 (2000), https://doi.org/10.1063/1.481405.

[11] I. Rahinov, Y. Toker, O. Heber, D. Strasser, M. Rappaport, D. Schwalm, and D. Zajfman, Review of Scientific Instruments **83**, 033302 (2012), https://doi.org/10.1063/1.3694997.

[12] A. Langdon and C. K. Birdsall, *Plasma Physics via Computer Simulation, 1st ed.* (CRC Press, 1985).

[13] R. Ringle, International Journal of Mass Spectrometry

303, 42 (2011).
[14] R. Ringle, G. Bollen, K. Lund, C. Nicoloff, S. Schwarz, C. Sumithrarachchi, and A. Villari, Nuclear Instruments and Methods in Physics Research Section B: Beam Interactions with Materials and Atoms **496**, 61 (2021).
[15] C. K. Birdsall and D. Fuss, Journal of Computational Physics **3**, 494 (1969).
[16] M. Lai, W. Lin, and W. Wang, IMA Journal of Numerical Analysis **22**, 537 (2002), https://academic.oup.com/imajna/article-pdf/22/4/537/2649564/220537.pdf.
[17] D. A. Dahl, International Journal of Mass Spectrometry **200**, 3 (2000).
[18] E. N. Nikolaev, R. M. A. Heeren, A. M. Popov, A. V. Pozdneev, and K. S. Chingin, Rapid Communications in Mass Spectrometry **21**, 3527 3546 (2007).
[19] H. B. Pedersen, D. Strasser, O. Heber, M. L. Rappaport, and D. Zajfman, Phys. Rev. A **65**, 042703 (2002).
[20] D. Zajfman, Y. Rudich, I. Sagi, D. Strasser, D. Savin, S. Goldberg, M. Rappaport, and O. Heber, International Journal of Mass Spectrometry **229**, 55 (2003), mass Spectrometry Contributions to Nanosciences and Nanotechnology.
[21] P. Fischer, S. Knig, and L. Schweikhard, International Journal of Mass Spectrometry **463**, 116546 (2021).
[22] W. C. Wiley and I. H. McLaren, Review of Scientific Instruments **26**, 1150 (1955), https://doi.org/10.1063/1.1715212.
[23] M. Guilhaus, Journal of Mass Spectrometry **30**, 1519 (1995).
[24] A. G. Marshall, C. L. Hendrickson, and G. S. Jackson, Mass Spectrometry Reviews **17**, 1 (1998).
[25] I. J. Amster, Journal of Mass Spectrometry **31**, 1325 (1996).
[26] I. Mardor, S. A. S. Andrés, T. Dickel, D. Amanbayev, S. Beck, J. Bergmann, H. Geissel, L. Gröf, E. Haettner, C. Hornung, N. Kalantar-Nayestanaki, G. Kripko-Koncz, I. Miskun, A. Mollaebrahimi, W. R. Plaß, C. Scheidenberger, H. Weick, S. Bagchi, D. L. Balabanski, A. A. Bezbakh, Z. Brencic, O. Charviakova, V. Chudoba, P. Constantin, M. Dehghan, A. S. Fomichev, L. V. Grigorenko, O. Hall, M. N. Harakeh, J.-P. Hucka, A. Kankainen, O. Kiselev, R. Knöbel, D. A. Kostyleva, S. A. Krupko, N. Kurkova, N. Kuzminchuk, I. Mukha, I. A. Muzalevskii, D. Nichita, C. Nociforo, Z. Patyk, M. Pfützner, S. Pietri, S. Purushothaman, M. P. Reiter, H. Roesch, F. Schirru, P. G. Sharov, A. Spătaru, G. Stanic, A. State, Y. K. Tanaka, M. Vencelj, M. I. Yavor, and J. Zhao, Phys. Rev. C **103**, 034319 (2021).
[27] M. Reiter, F. Ames, C. Andreoiu, S. Ayet San Andrs, C. Babcock, B. Barquest, J. Bergmann, J. Bollig, T. Brunner, T. Dickel, J. Dilling, I. Dillmann, E. Dunling, A. Finlay, G. Gwinner, L. Graham, C. Hornung, B. Kootte, R. Klawitter, P. Kunz, Y. Lan, D. Lascar, J. Lassen, E. Leistenschneider, R. Li, J. McKay, M. Mostamand, S. Paul, W. Pla, C. Scheidenberger, B. Schultz, R. Steinbrgge, A. Teigelhoefer, R. Thompson, M. Wieser, C. Will, and A. Kwiatkowski, Nuclear Instruments and Methods in Physics Research Section B: Beam Interactions with Materials and Atoms **463**, 431 (2020).
[28] D. Grinfeld, H. Stewart, M. Skoblin, E. Denisov, M. Monastyrsky, and A. Makarov, International Journal of Modern Physics A **34**, 1942007 (2019), https://doi.org/10.1142/S0217751X19420077.
[29] S. Ring, H. B. Pedersen, O. Heber, M. L. Rappaport, P. D. Witte, K. G. Bhushan, N. Altstein, Y. Rudich, I. Sagi, and D. Zajfman, Analytical Chemistry **72**, 4041 (2000).
[30] Z. Fradkin, D. Strasser, O. Heber, M. Rappaport, M. Sharon, B. Thomson, I. Rahinov, Y. Toker, and D. Zajfman, Journal of Instrumentation **12**, P05008 (2017).
[31] P. Bolotskikh, D. Grinfeld, A. Makarov, and M. Monastyrskiy, Nuclear Instruments and Methods in Physics Research Section A: Accelerators, Spectrometers, Detectors and Associated Equipment **645**, 146 (2011), the Eighth International Conference on Charged Particle Optics.
[32] A. Savitzky and M. J. E. Golay, Analytical Chemistry **36**, 1627 (1964), https://doi.org/10.1021/ac60214a047.
[33] N. Otsu, IEEE Transactions on Systems, Man, and Cybernetics **9**, 62 (1979).
[34] H. A. Sturges, Journal of the American Statistical Association **21**, 65 (1926), https://doi.org/10.1080/01621459.1926.10502161.